Title	Submillimeter array observation of the proto-planetary nebula CRL 618 in the CO J = 6-5 line
Author(s)	Nakashima, JI; Fong, D; Hasegawa, T; Hirano, N; Koning, N; Kwok, S; Lim, J; DinhVanTrung; Young, K
Citation	Astronomical Journal, 2007, v. 134 n. 5, p. 2035-2045
Issued Date	2007
URL	http://hdl.handle.net/10722/57330
Rights	Creative Commons: Attribution 3.0 Hong Kong License

The Astronomical Journal, 134:2035–2045, 2007 November

SUBMILLIMETER ARRAY OBSERVATION OF THE PROTO–PLANETARY NEBULA CRL 618 IN THE CO $J = 6$–5 LINE

Jun-ichi Nakashima,[1] David Fong,[2] Tatsuhiko Hasegawa,[1] Naomi Hirano,[1] Nico Koning,[3] Sun Kwok,[1,4] Jeremy Lim,[1] Dinh-Van-Trung,[1] and Ken Young[5]
Received 2007 June 20; accepted 2007 July 26

ABSTRACT

We report on the results of a Submillimeter Array (SMA) interferometric observation of the proto–planetary nebula CRL 618 in the ^{12}CO $J = 6$–5 line. With the new capability of the SMA enabling us to use two receivers at a time, we also observed simultaneously in the ^{12}CO $J = 2$–1 and ^{13}CO $J = 2$–1 lines. The ^{12}CO $J = 6$–5 and ^{13}CO $J = 2$–1 lines were interferometrically observed for the first time toward CRL 618. The flux of the high-velocity component of the ^{12}CO $J = 6$–5 line is almost fully recovered, while roughly 80% of the flux of the low-velocity component is resolved out. The low recovery rate suggests that the emission region of the low-velocity component of the ^{12}CO $J = 6$–5 line is largely extended. Continuum emission is detected at both 230 and 690 GHz. The flux of the 690 GHz continuum emission seems to be partially resolved out, suggesting that dust emission partly contaminates the 690 GHz continuum flux. The cavity structure, which has been confirmed in a previous observation in the ^{12}CO $J = 2$–1 line, is not clearly detected in the ^{12}CO $J = 6$–5 line, and only the south wall of the cavity is detected. This result suggests that the physical condition of the molecular envelope of CRL 618 is not exactly axially symmetric.

Key words: stars: AGB and post-AGB — stars: carbon — stars: imaging — stars: individual (CRL 618) — stars: kinematics — stars: winds, outflows

1. INTRODUCTION

Stellar evolution from the asymptotic giant branch (AGB) phase to the planetary nebula (PN) phase is very rapid. This transient phase between the AGB and PN phases is often called the proto–planetary nebula (PPN) phase and/or post-AGB phase (Kwok 1993; van Winckel 2003). PPNe are considered to play an important role in a wide variety of astrophysical problems: for example, the shape and shaping of PNe, the chemical evolution of the evolved stars, and the synthesis of organic matter in space (Balick & Frank 2002; Kwok 2004). Unfortunately, however, the number of PPNe identified is rather limited, mainly due to their transient existence (see, e.g., Szczerba et al. 2007).

In the last few decades, the well-known example of a PPN, CRL 618 (= RAFGL 618 = IRAS 04395+3601 = Westbrook Nebula), has provided a unique opportunity to investigate the nature of at least one particular case of PPNe. CRL 618 entered its PPN phase about 100 yr ago (Kwok & Bignell 1984), and the central B0 star is surrounded by a compact H II region (its angular size is roughly $0.2'' \times 0.4''$) visible through centimeter- and millimeter-wave continuum emission (Wynn-Williams 1977; Kwok & Feldman 1981; Kwok & Bignell 1984; Martín-Pintado 1993). The flux of the free-free emission at $\lambda = 1.3$ and 3 mm has been continuously changing over the last 25 yr (see, e.g., Sánchez Contreras et al. 2004), implying the rapid evolution of this object. The envelope of CRL 618 includes a rich set of molecular species (e.g., Bujarrabal et al. 1988; Cernicharo et al. 1989, 2001a, 2001b; Fukasaku et al. 1994; Remijan et al. 2005), and has been repeatedly observed in molecular radio lines, especially that of CO (e.g., Shibata et al. 1993; Yamamura et al. 1994; Hajian et al. 1996; Sánchez Contreras et al. 2004).

Through radio observations in molecular rotational lines, four different kinematical components have been identified in the molecular envelope of CRL 618. In Figure 1 we present a schematic view of the molecular envelope of CRL 618. The first component [corresponding to (1) in Fig. 1] exhibits an almost round shape in CO maps, and its angular size is larger than 20″. The expanding velocity of this spherical component is roughly 17.5 km s^{-1}, and it is interpreted as the remnant of the spherical mass-loss process of the central star during the AGB phase. The second component [corresponding to (2) in Fig. 1] exhibits a bipolar flow observed up to axial distances of $\pm 2.5''$ from the nebula center. The expansion velocity of this component reaches up to 350 km s^{-1}. Incidentally, the proper motion of this high-velocity bipolar flow has been measured by Sánchez Contreras & Sahai (2004), and the value is $\sim 0.045''$ yr^{-1}, corresponding to a distance of 900 pc if we assume the inclination angle of the polar axis is 30°; this distance is consistent with that estimated by an independent method (Goodrich 1991). An additional two kinematical components were recently found by Sánchez Contreras et al. (2004) in their high-resolution ($\sim 1''$) interferometric radio observation: an extended structure elongated in the polar direction up to an axial distance of $\pm 6''$ from the nebula center, which is expanding at a velocity of about 22 km s^{-1} [corresponding to (3) in Fig. 1], and a dense, inner torus-like core expanding at a velocity of less than 12 km s^{-1} [corresponding to (4) in Fig. 1].

Although numerous observational and theoretical efforts have been made for CRL 618, several interesting puzzles remain. First, the largely extended torus-like structure is detectable in the HCO$^+$ $J = 1$–0 line, but not in the CO $J = 2$–1 line (Sánchez Contreras et al. 2004; Sánchez Contreras & Sahai 2004). Sánchez Contreras et al. (2004) suggested that a passage of a shock across the torus-like structure plays an important role in explaining this

[1] Academia Sinica Institute of Astronomy and Astrophysics, P.O. Box 23-141, Taipei 106, Taiwan; junichi@asiaa.sinica.edu.tw.
[2] Submillimeter Array, Harvard-Smithsonian Center for Astrophysics, 645 North A'ohoku Place, Hilo, HI 96720, USA.
[3] Department of Physics and Astronomy, University of Calgary, Calgary, AB T2N 1N4, Canada.
[4] Faculty of Science, University of Hong Kong, Chong Yuet Ming Physics Building, Hong Kong, China.
[5] Harvard-Smithsonian Center for Astrophysics, 60 Garden Street, Cambridge, MA 02138, USA.

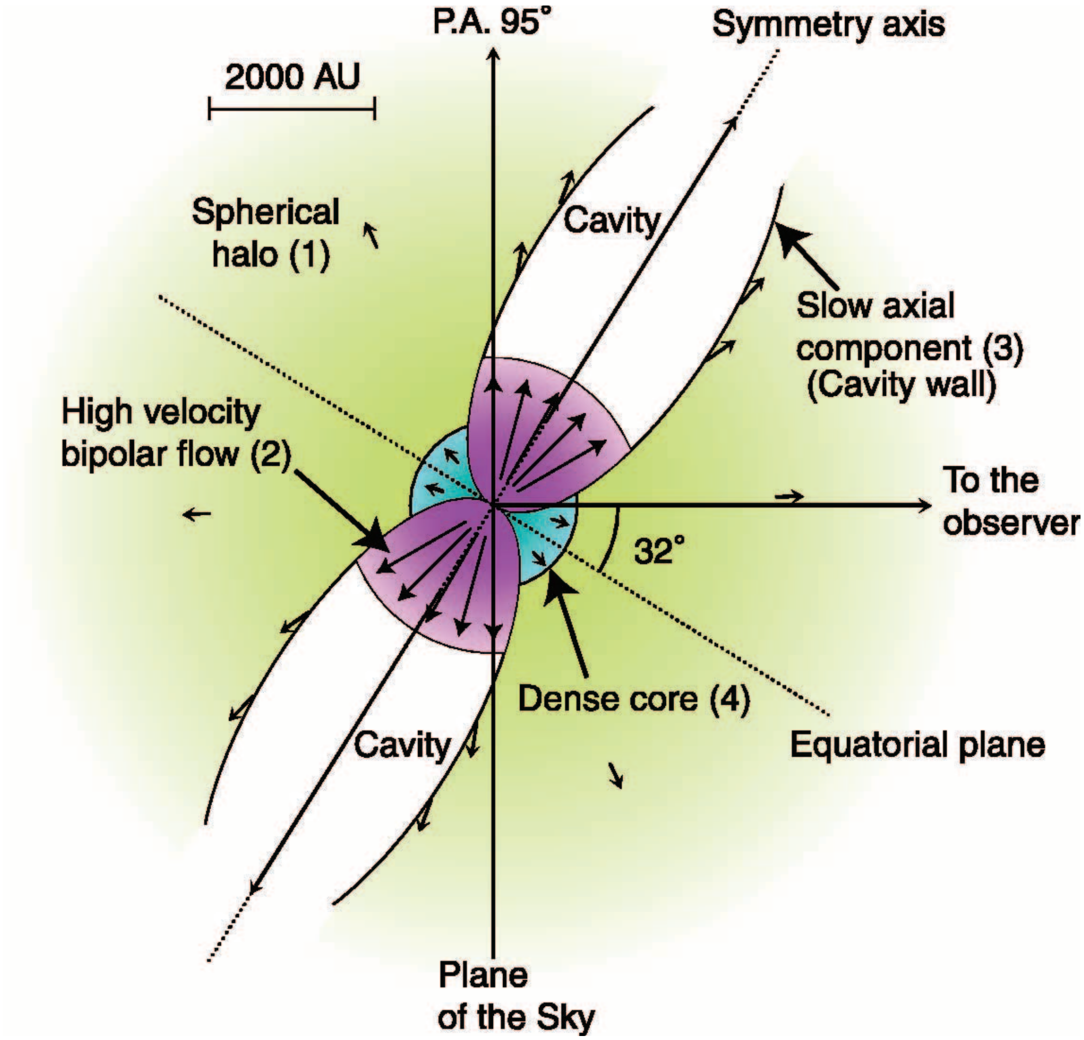

Fig. 1.—Schematic view of the molecular envelope of CRL 618 made using examples from Fig. 5 in Sánchez Contreras et al. (2004). The small arrows indicate the velocity field of the envelope. The numbers in parentheses correspond to the numbers of the components referred to in the text (see § 1).

phenomenon. Second, the light curve of the intensity of the free-free emission has exhibited a sudden increase over the past 5 yr (Sánchez Contreras et al. 2004), implying that CRL 618 exhibits the activity of a post-AGB wind, which is very poorly understood (e.g., Bujarrabal et al. 1994; Jura & Chen 2000; Steffen et al. 2001; García-Segura et al. 2005). Third, the molecular envelope of CRL 618 exhibits a hybrid chemistry, simultaneously including both oxygen- and carbon-rich environments (e.g., Bujarrabal et al. 1988; Cernicharo et al. 1989). Such a mixture of C/O-rich chemistry has been recognized in some late-type stars (e.g., CRL 2688, OH 231.8+4.2, and IRAS 19312+1950; Lucas et al. 1986; Morris et al. 1987; Nakashima & Deguchi 2000, 2004, 2005; Murakawa et al. 2007), but the origin of the mixture is still unclear.

Further observations of CRL 618, especially using new instruments with new capabilities, would be valuable in understanding the nature of this interesting object. In this paper we report the first results of a Submillimeter Array[6] (SMA) interferometric observation of CRL 618 in the ^{12}CO $J = 6$–5 line, using the new capability of the SMA to observe at 690 GHz. This observation has been made as a part of the SMA 690 GHz observation campaign. In addition to the ^{12}CO $J = 6$–5 line, we briefly report the results of observations in other molecular lines, including the ^{12}CO $J = 2$–1 and ^{13}CO $J = 2$–1 lines. The outline of the paper is as follows: In § 2 details of the observations and data reduction are presented. In § 3 results of the observation are presented, including spectra and intensity maps of the CO lines, intensity and position measurements of the continuum emission, and identification of the detected molecular lines. In § 4 we discuss the properties of the ^{12}CO $J = 6$–5 line. Finally, the results of the present observation are summarized in § 5.

2. DETAILS OF OBSERVATIONS AND DATA REDUCTION

Interferometric observations of CRL 618 were made with the SMA on 2005 February 18. Data were obtained under very good atmospheric conditions with a zenith optical depth at 230 GHz of 0.05 on average. The instrument has been described in detail by Ho et al. (2004) and Ohashi (2005). With the capability of the SMA of using two different receivers at a time, we observed simultaneously in four different frequency bands: 690.572–692.549, 680.572–682.550, 219.598–221.575, and 229.600–231.576 GHz. These frequency ranges cover three CO lines: the ^{12}CO $J = 6$–5, ^{12}CO $J = 2$–1, and ^{13}CO $J = 2$–1 lines.

[6] The Submillimeter Array is a joint project between the Smithsonian Astrophysical Observatory and the Academia Sinica Institute of Astronomy and Astrophysics, and is funded by the Smithsonian Institution and the Academia Sinica.

The array used six elements (with a diameter of 6 m) in the compact array configuration. The baseline length ranged from 10 to 70 m. The field of view of a single antenna was 18″ and 54″ at 690 and 230 GHz, respectively. The observation was interleaved every 15 minutes with nearby gain calibrators, 3C 111 and Titan, to track the phase variations over time. Because the angular size of Titan was roughly $0.88'' \times 0.68''$, Titan was not an ideal point source compared with the small size of the beam ($\sim$1″–3″) of the present observations. Therefore, in the gain calibration we used the `non-point` flag of the `gain-cal` command in the IDL-MIR package, which enabled us to use a planet/satellite as a calibrator (IDL-MIR is data reduction software developed by the SMA project). The `non-point` flag function assumes the calibrator is a uniform disk; the size and flux of the calibrator are automatically retrieved and calculated by the internal theoretical calculation. The absolute flux calibration was determined from observations of Ganymede, and was approximately accurate to within 15%. We adopted the antenna-based solution in the passband calibration of the 690 GHz data. With enough signal-to-noise ratio in each channel, the antenna-based bandpass solution is robust and consistent with baseline-based calibration results. For the 230 GHz data we adopted a standard calibration method using the baseline-based solution. The final map has an accumulated on-source observing time of about 4 hr. The single-sideband system temperature ranged from 2000 to 3000 K at 690 GHz and from 150 to 200 K at 230 GHz, depending on the atmospheric conditions and the telescope direction. The SMA correlator had a bandwidth of 2 GHz with a resolution of 0.812 MHz. The velocity resolution was 0.35 km s^{-1} at 690 GHz and 1.0 km s^{-1} at 230 GHz. The phase center of the map was taken at R.A. $= 04^{h}42^{m}53.67^{s}$, decl. $= 36°06'53.2''$ (J2000.0). Image processing of the data was performed with the MIRIAD software package (Sault et al. 1995). We used robust weighting for the 690 GHz data. The robust weighting of the visibility data, which is an optimized compromise between natural and uniform weighting, gave a $1.0'' \times 0.8''$ CLEAN beam at 690 GHz with a position angle of $-12°$. For the ^{12}CO and ^{13}CO $J = 2$–1 lines, a superuniform weighting of visibility data (with a suppression region of $8'' \times 8''$) was adopted to enhance the angular resolution, and this weighting gave a $2.6'' \times 2.4''$ CLEAN beam with a position angle of $+11.2°$. The widths of the bands for the continuum maps at 690 and 230 GHz were roughly 1.5 and 1.9 GHz, respectively.

3. RESULTS

3.1. *Spectra of the* CO *Lines*

Figure 2 shows the spatially integrated spectra of the observed CO lines. The line emission was integrated over a circular region with a diameter of 15″. The continuum flux was calculated in the line-free channels, and the continuum emission was subtracted from the spectra to retrieve only the line emission. As reported in previous papers, the ^{12}CO $J = 2$–1 line clearly shows two different components (i.e., a high-velocity pedestal component and a low-velocity strong component; see, e.g., Bujarrabal et al. 1988, 2001; Cernicharo et al. 1989; Neri et al. 1992; Meixner et al. 1998; Sánchez Contreras et al. 2004; Sánchez Contreras & Sahai 2004). In comparison with a single-dish spectrum (Bujarrabal et al. 1988), there is no significant loss of the flux in the high-velocity component of the ^{12}CO $J = 2$–1 line, but roughly 45% of the flux of the low-velocity component is resolved out. In fact, the line profile of the high-velocity component of the ^{12}CO $J = 2$–1 line is quite similar to that obtained in previous single-dish observations, but the peak intensity of the low-velocity component is clearly lower than values of the single-dish measurements.

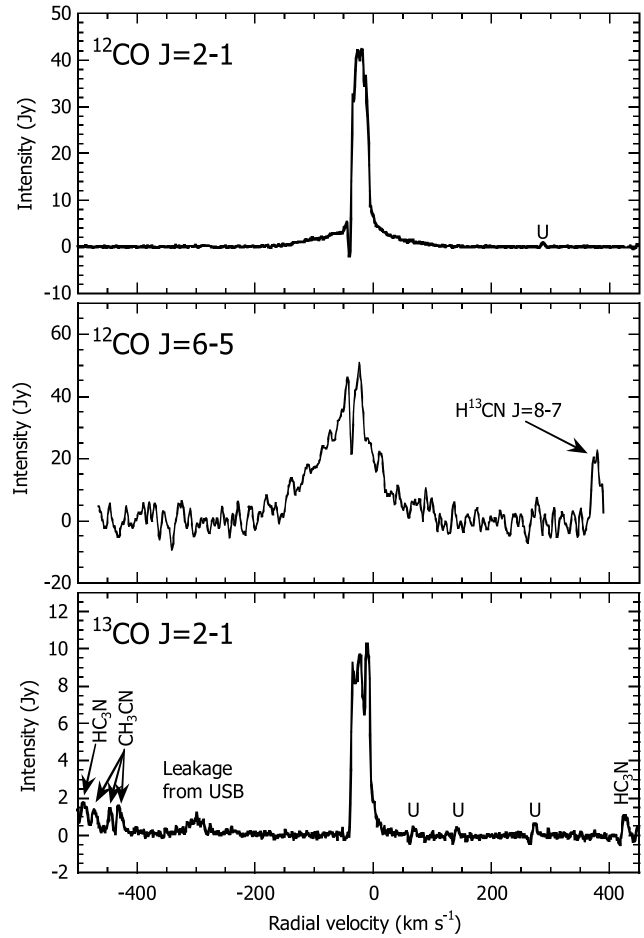

FIG. 2.—Spatially integrated spectra of the ^{12}CO $J = 2$–1, ^{12}CO $J = 6$–5, and ^{13}CO $J = 2$–1 lines. The integrated area is a circle with an angular diameter of 15″. For the ^{12}CO $J = 6$–5 line, the spectrum is smoothed over every 5 km s^{-1}. The other detected lines seen in the spectra are indicated by the name of the molecular species or by "U," meaning an unidentified line.

The ^{12}CO $J = 6$–5 and ^{13}CO $J = 2$–1 lines have been interferometrically observed for the first time, and at a glance, these lines exhibit different line profiles compared with the ^{12}CO $J =$ 2–1 line. The high-velocity component of the ^{12}CO $J = 6$–5 line is clearly detected, exhibiting the maximum line width of about 350 km s^{-1} at the zero-intensity level, while the low-velocity component is relatively weak. This weak intensity seems to be caused by missing flux resolved out by the interferometry. In fact, the peak intensity of the ^{12}CO $J = 6$–5 line measured by a single-dish observation is 320 Jy (Herpin et al. 2002), while the peak intensity of the ^{12}CO $J = 6$–5 line measured in the present observation is 55.3 Jy. In comparison with Herpin's single-dish observation, roughly 80% of the flux of the low-velocity component of the ^{12}CO $J = 6$–5 line is resolved out in the present observation, even though there is no significant missing flux in the high-velocity component of the ^{12}CO $J = 6$–5 line. The large amount of missing flux of the low-velocity component implies that the emission region of the low-velocity component of the ^{12}CO $J = 6$–5 line is largely extended.

The ^{13}CO $J = 2$–1 line exhibits only the low-velocity component, presumably related to the sensitivity. In comparison with a single-dish observation (Bujarrabal et al. 1988), there is

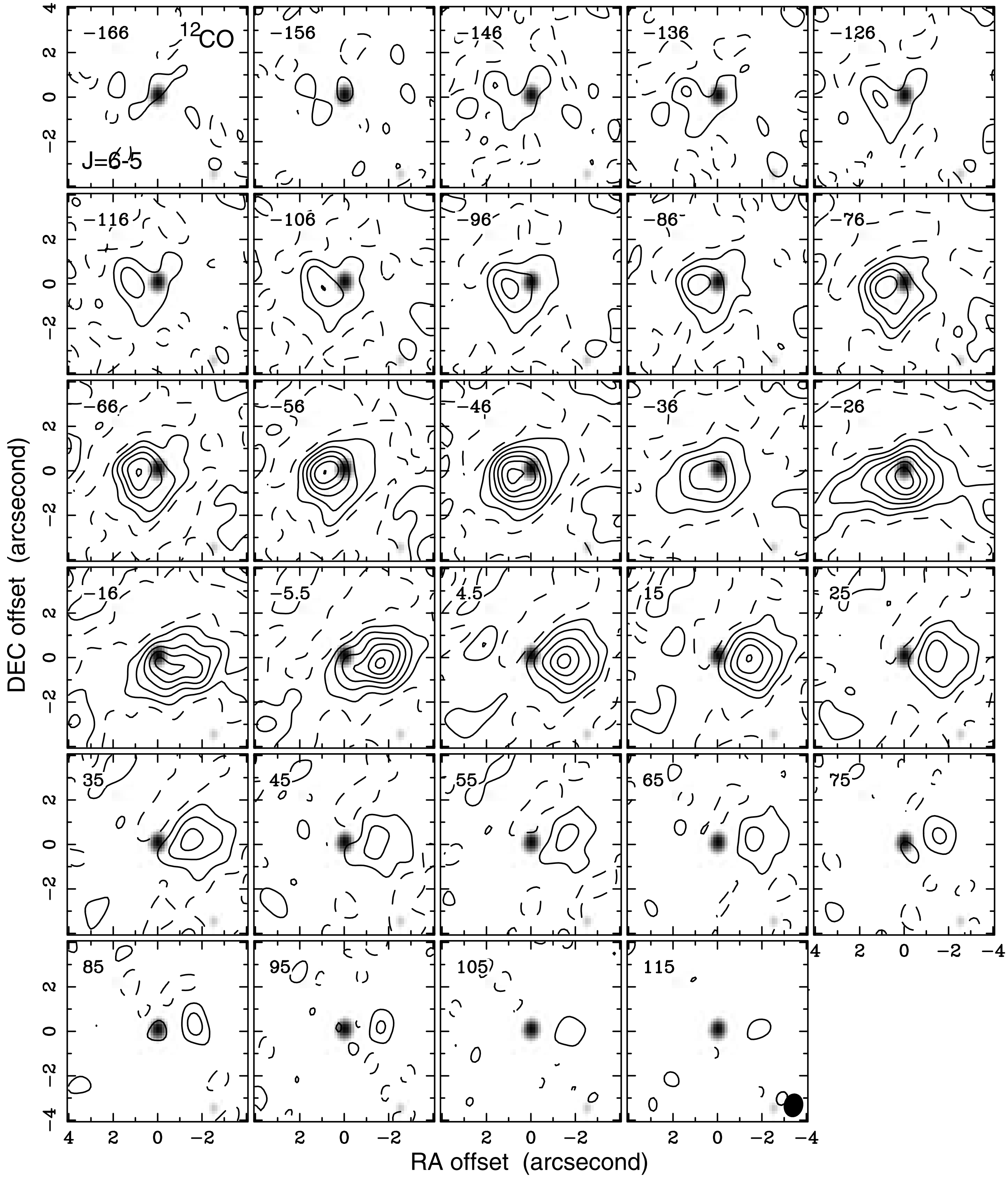

Fig. 3.—Velocity channel maps of the CO $J = 6$–5 line. The velocity channels are averaged over 10 km s^{-1} intervals. The contours start from the 3 σ level, and the levels are spaced every 5 σ. The 1 σ level corresponds to 4.42×10^{-1} Jy beam^{-1}. The dashed contour corresponds to -3 σ. The peak intensity corresponds to 28 σ. The synthesized beam is indicated in the bottom right panel. The background gray scale represents the intensity of the 690 GHz continuum emission.

no significant flux loss in the low-velocity component of the ^{13}CO $J = 2$–1 line. In all three spectra of the CO lines, we can see an absorption feature at $V_{\rm lsr} \sim -40$ km s^{-1}. Although it is somewhat difficult to see the absorption feature in the ^{13}CO $J = 2$–1 line (at least, there is no absorption below the continuum level), the line profile of the ^{13}CO $J = 2$–1 line is certainly asymmetric: it shows a weaker blue side compared with the red one (this is clearly seen in the p-v diagram given in a later section; see Fig. 8). Therefore, there is in fact absorption of the blue side of the low-velocity component in the ^{13}CO $J = 2$–1 line. The profile of the low-velocity component, showing a spiky feature, is somewhat different from that of the ^{12}CO $J = 2$–1 line, showing a parabolic profile. This difference is presumably due to the relatively thin optical depth of the ^{13}CO $J = 2$–1 line. The spiky profile suggests a complex kinematics in the inner part the molecular envelope. In Figure 2 (*bottom*) we can see a broad emission feature at $V_{\rm lsr} \sim -300$ km s^{-1}, which can be explained by leakage of the strong ^{12}CO $J = 2$–1 line lying in the other sideband. This conclusion is based on the fact that the peak velocity of this feature exactly corresponds to the backside of the ^{12}CO $J = 2$–1 line, the line profile is very similar to that of the ^{12}CO $J = 2$–1 line, and also because no possible lines are found in molecular line catalogs. (Note that this leakage problem has already been fixed, and the current SMA system has no problems even in the case of very strong lines such as CO lines.)

3.2. *Intensity Maps of* CO *Lines*

Figure 3 shows the velocity channel maps of the ^{12}CO $J =$ 6–5 line. The background gray scale represents the continuum emission at 690 GHz, and the origin of the map is taken at the intensity peak of the continuum emission. In Figure 3 we can clearly see a velocity gradient in the east-west direction, as well as in the ^{12}CO $J = 2$–1 map by Sánchez Contreras et al. (2004). Interestingly, we cannot see the cavity structure found by Sánchez Contreras et al. (2004) in the ^{12}CO $J = 2$–1 line, although the angular resolution of the present observation in the ^{12}CO $J = 6$–5 line roughly equals that of Sánchez Contreras's observation in the ^{12}CO $J = 2$–1 line. Both ends of the high-velocity component (i.e., from -166 to -116 km s^{-1} and from 35 to 115 km s^{-1}) are clearly extended in the east-west direction up to roughly $\pm 2.5''$ from the nebula center. This size of the extension in the east-west direction is the same as that seen in the ^{12}CO $J = 2$–1 line.

In Figure 4 we present the velocity-integrated intensity maps of the ^{12}CO $J = 6$–5 line superimposed on the *HST* WFPC2 Hα + continuum image (Trammell & Goodrich 2002). The cross indicates the intensity peak of the radio continuum emission at 690 GHz. The direction of the elongation of the ^{12}CO $J = 6$–5 feature coincides with that of the optical feature seen in the *HST* image. The emission region of the high-velocity component of the ^{12}CO $J = 6$–5 line is limited to the optically faint region (i.e., the vicinity of the nebula center). In comparison with the maps in Sánchez Contreras et al. (2004), the spatial size of the emission region of the low-velocity component of the ^{12}CO $J = 6$–5 line is smaller than that of the ^{12}CO $J = 2$–1 line. This small size is due presumably to the large missing flux.

Figure 5 shows the channel velocity maps of the ^{13}CO $J =$ 2–1 line. In contrast to the ^{12}CO $J = 6$–5 line, the velocity gradient is not clear. This is due to a low signal-to-noise ratio in the high-velocity component of the ^{13}CO $J = 2$–1 line. In Figures 6 and 7 we present the velocity channel maps of the ^{12}CO $J =$ 2–1 line. We present the maps of the low-velocity component in Figure 6, and also present those of the high-velocity component in Figure 7. The features of the ^{12}CO $J = 2$–1 line seen in Figures 6 and 7 are in good agreement with the maps given by Sánchez Contreras et al. (2004); we can clearly see a velocity gradient in the east-west direction. The cavity structure seen in Sánchez Contreras's maps is not clear in Figure 6. This is due to the low angular resolution of the present observation. In Figure 7 both ends of the high-velocity component are extended in the east-west direction up to $\pm 2.5''$ from the nebular center. This is also consistent with the results of Sánchez Contreras et al. (2004). We cannot see the spherical halo seen in the Sánchez

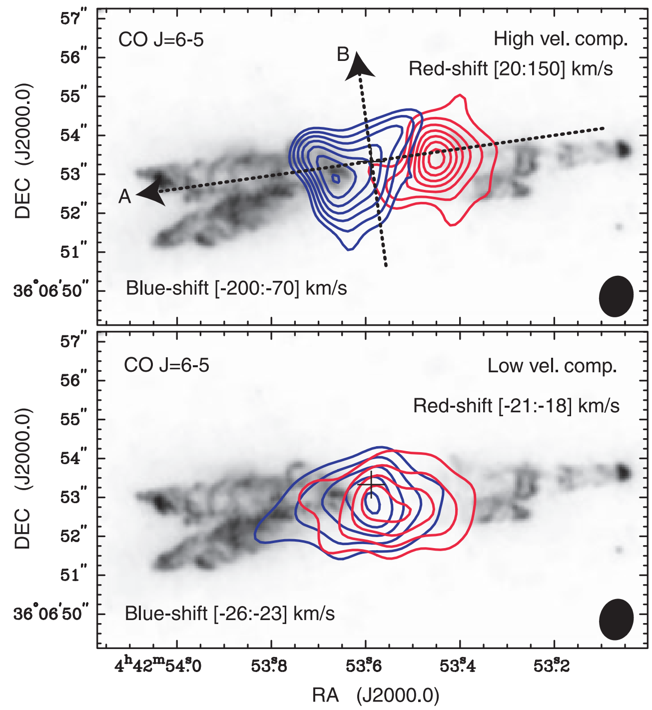

FIG. 4.—Velocity-integrated intensity maps of the CO $J = 6$–5 line superimposed on the *HST* WFPC2 Hα + continuum image (Trammell & Goodrich 2002). The red and blue contours represent the redshifted and blueshifted parts of the high- and low-velocity components. The velocity ranges of the integration are given in the panels. The lowest contour corresponds to the 3 σ level, and the levels are spaced every 4 σ; the 1 σ levels for the top and bottom panels are 1.2×10^{-1} and 6.9×10^{-1} Jy beam^{-1}, respectively. The synthesized beam size is given in the lower right corner. The dotted arrows A and B indicate the directions along which the *p*-*v* cuts shown in Fig. 8 were taken.

Contreras maps due to a lack of sensitivity. In fact, the 1 σ level in Figure 2*b* in Sánchez Contreras et al. (2004) is 45 mJy beam^{-1} (the beam size is $1.1'' \times 0.9''$); in contrast, the 1 σ level in Figure 6 is 100 mJy beam^{-1} (the beam size is $3.3'' \times 2.8''$). Missing flux, in principle, could be a reason for the absence, but we recovered 55% of the flux of the low-velocity component, and this recovery rate is larger than the 40% of Sánchez Contreras's observation.

For a better understanding of the kinematical properties, we present position-velocity (*p*-*v*) diagrams in Figure 8. The present data are superimposed on the *p*-*v* diagram of the ^{12}CO $J = 2$–1 line taken from Sánchez Contreras et al. (2004). The left and right columns represent *p*-*v* diagrams in the axial and perpendicular directions, respectively. In the middle two panels, we can see that the emission of the ^{12}CO $J = 2$–1 line is not detected in the high-velocity ends due to a lack of sensitivity. The features of the ^{12}CO $J = 6$–5 line are basically consistent with those of the ^{12}CO $J = 2$–1 line, even though the spatial size of the low-velocity component of the ^{12}CO $J = 6$–5 line is smaller than that of the ^{12}CO $J = 2$–1 line.

3.3. *Continuum Emission*

The continuum emission of CRL 618 was detected at both 230 and 690 GHz. The continuum emission at 690 GHz has been interferometrically observed for the first time. These continuum emissions seem to exhibit a pointlike feature in the intensity maps, but the *u*-*v* distance versus amplitude plot of the 690 GHz continuum emission shows that the amplitude increases with decreasing *u*-*v* distance (although we do not present the plot

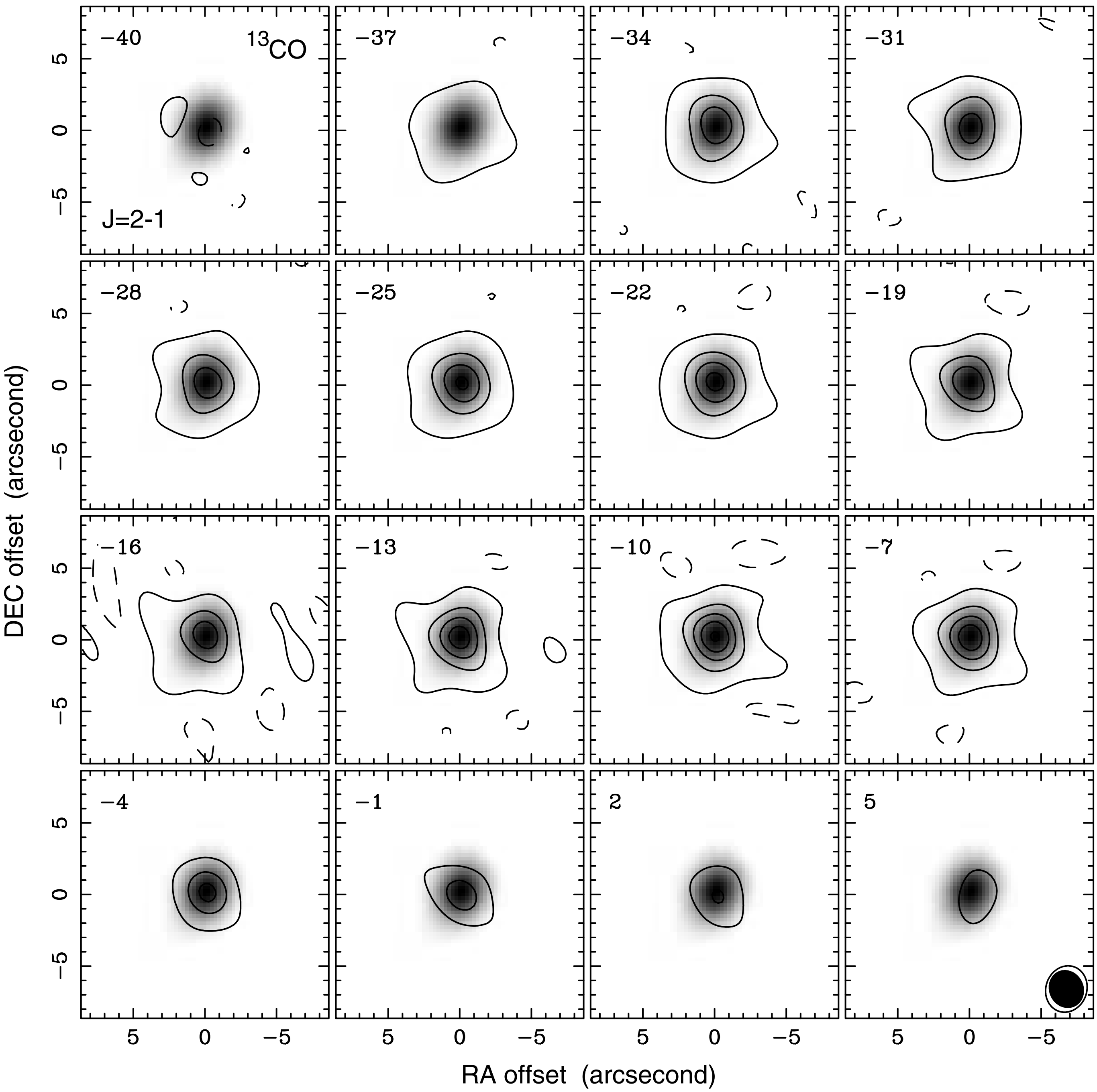

Fig. 5.—Velocity channel maps of the ^{13}CO $J = 2$–1 line. The velocity channels are averaged over 3 km s^{-1} intervals. The contours start from the 3 σ level, and the levels are spaced every 10 σ. The 1 σ level corresponds to 9.5×10^{-2} Jy beam^{-1}. The dashed contour corresponds to -3 σ. The intensity peak corresponds to 40 σ. The background gray scale represents the intensity of the 1 mm continuum emission. The synthesized beam is indicated in the bottom right panel; the outer open and inner filled ellipses represent the beam sizes for the line and continuum maps, respectively.

here), suggesting the 690 GHz continuum flux is partially resolved out. The integrated fluxes of the continuum emission are 2.0 and 2.7 Jy at 230 and 690 GHz, respectively. The 230 GHz continuum flux is consistent with the latest measurement by Sánchez Contreras et al. (2004). The spectral index calculated by the 230 and 690 GHz measurements is $\nu^{0.3}$. This is not consistent with the spectral index expected from optically thin free-free emission ($\nu^{-0.1}$). Incidentally, the turn-off point of the spectrum of the central H II region is roughly at 45 GHz (Knapp et al. 1993). Because the angular size of the central ionized region is $0.2'' \times 0.4''$, the free-free emission is not expected to be resolved by our synthesized beam. Therefore, the extended feature in the 690 GHz continuum emission presumably originates in the dust component in the envelope. The positions of the intensity peak of the continuum emission measured by a two-dimensional Gaussian function fitting are $4^{\rm h}42^{\rm m}53.58^{\rm s}$, $36^\circ06'53.4''$ (J2000.0) at 230 GHz (FWHM and position angle are $3.27'' \times 2.84''$ and -19.2°, respectively), and $4^{\rm h}42^{\rm m}53.59^{\rm s}$, $36^\circ06'53.3''$ (J2000.0) at 690 GHz (FWHM and position angle are $1.07'' \times 0.88''$ and -13.0°, respectively). These positions coincide well with that determined by a low-frequency observation (Wynn-Williams 1977) but are slightly shifted from the intensity peak of the CO $J = 6$–5 emission. (See Fig. 4, *bottom*; we discuss this matter below in § 4).

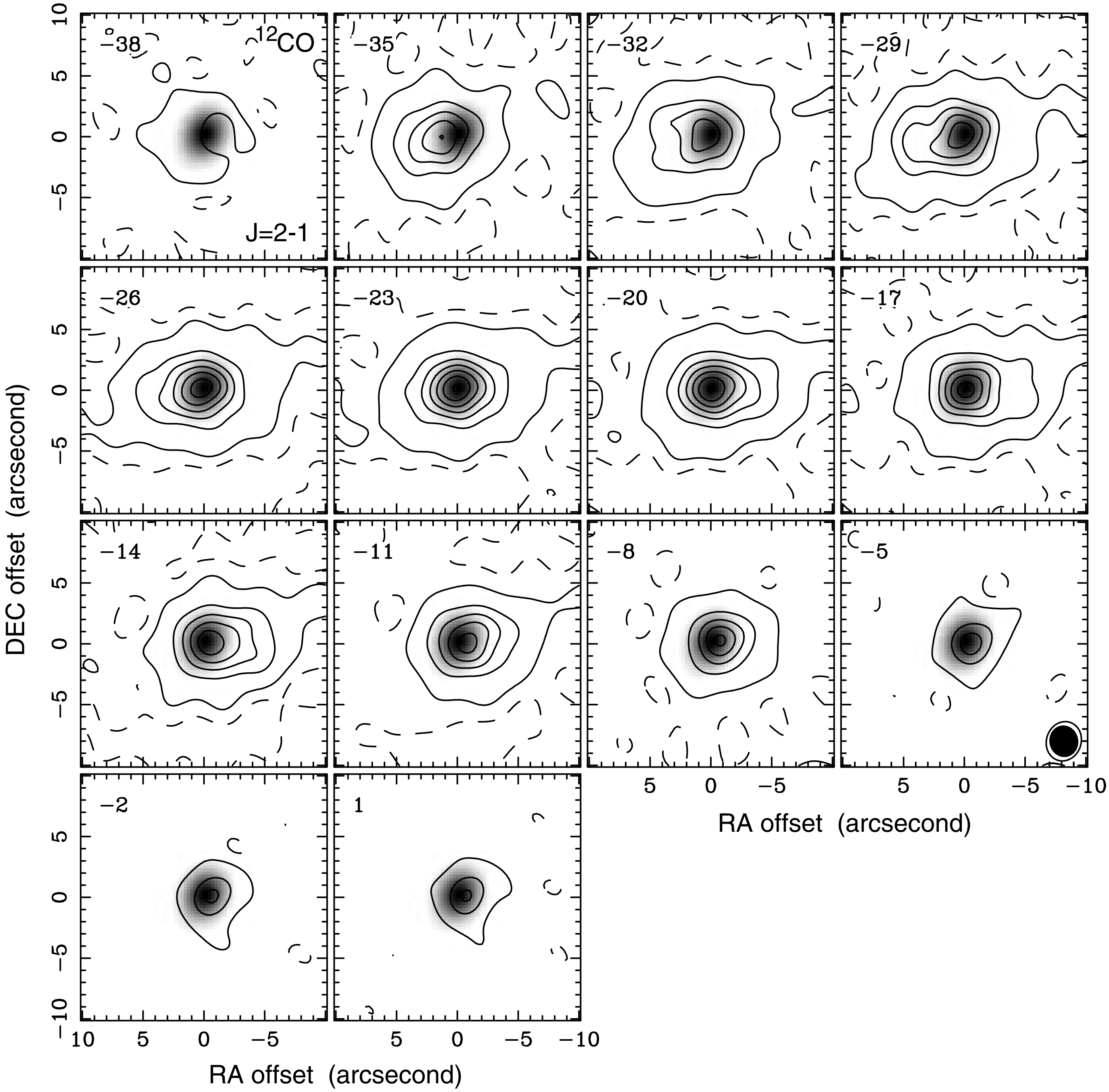

Fig. 6.—Velocity channel maps of the low-velocity component of the CO $J = 2$–1 line. The channel velocities are given in the upper left corner of each panel. The velocity channels were averaged over 1 km s^{-1} intervals. The contours start from the 3 σ level, and the levels are spaced every 20 σ. The dashed contour corresponds to -3 σ. The 1 σ level corresponds to 1.03×10^{-1} Jy beam^{-1}. The peak intensity corresponds to 120 σ. The background gray scale represents the intensity of the 1 mm continuum emission. The synthesized beam is indicated in the bottom right panel; the outer open and inner filled ellipses represent the beam sizes for the line and continuum maps, respectively.

3.4. *Other Detected Lines*

In Figure 9 we present a spectrum including all lines detected in the 230 GHz bands. The continuum emission was subtracted in Figure 9. In total we have detected 36 emission lines above the 5 σ level, and 24 out of the 36 detected lines are identified as known molecular lines. We used WinSpectra, the line identification software developed by the ODIN group at the University of Calgary, to identify the lines. WinSpectra uses the JPL and Cologne Database for Molecular Spectroscopy catalogs (Müller et al. 2001, 2005; Pearson et al. 2005) in a built-in form to retrieve the molecular data. The results of the line identification are summarized in Table 1. Most lines seen in Figure 9 exhibit a P Cygni profile, as reported in previous observations (Bujarrabal et al. 1988; Wyrowski et al. 2003; Pardo et al. 2004; Pardo & Cernicharo 2007). This suggests that most of the detected lines originate from an expanding and accelerating molecular envelope (see, e.g., Wyrowski et al. 2003). The frequencies in Table 1 represent the rest frequencies (for identified lines) or laboratory-frame frequencies, corrected using $V_{\rm lsr} = -23$ km s^{-1} (for

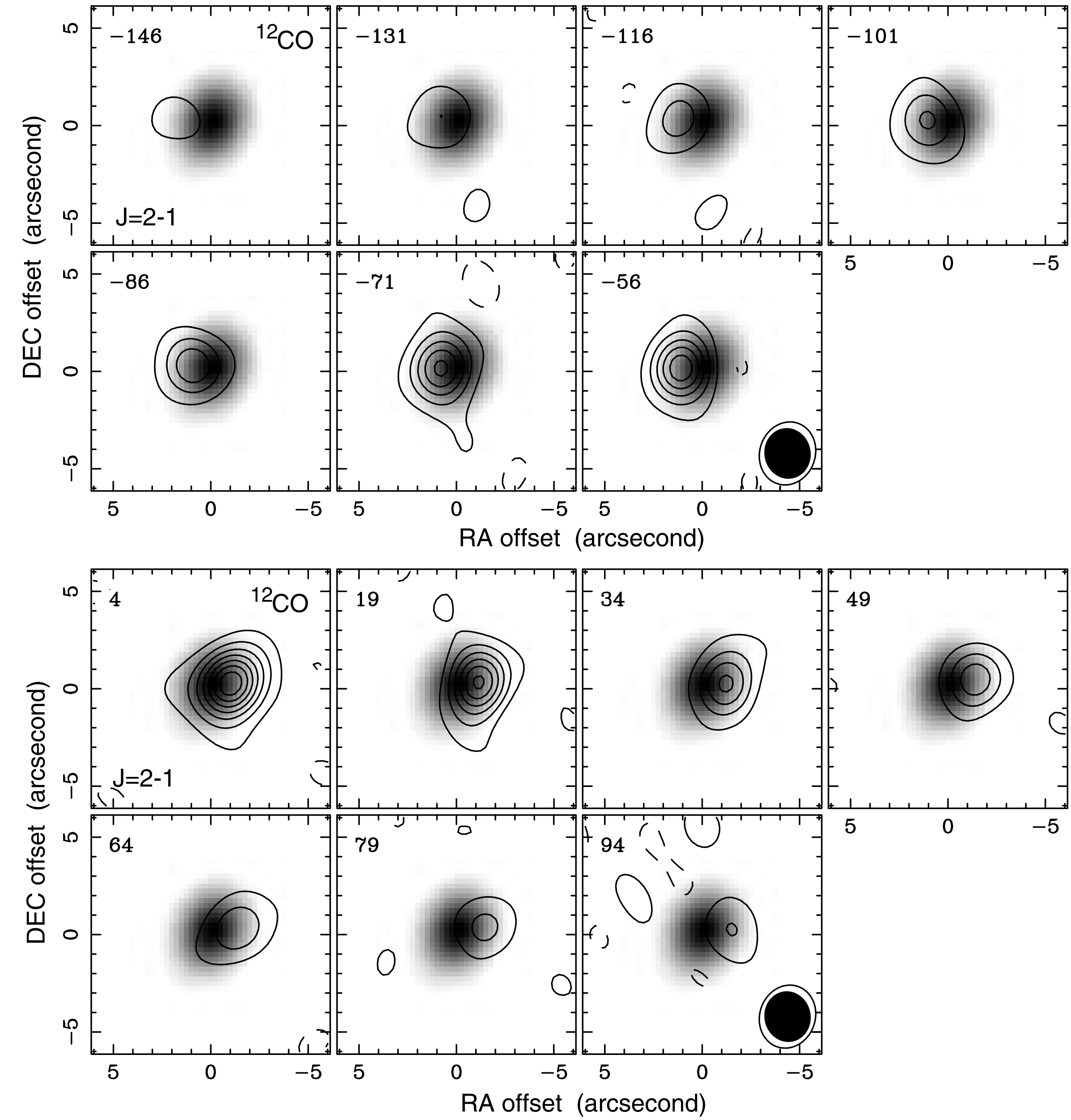

FIG. 7.—Velocity channel maps of the high-velocity component of the CO $J = 2$–1 line. The velocity channels are averaged over 1 km s^{-1} intervals. The contours start from the 3 σ level, and the levels are spaced every 10 σ. The dashed contour corresponds to $-3\ \sigma$. The 1 σ level, background gray scale, and synthesized beam are the same as in Fig. 6.

unidentified lines). "U" in Table 1 indicates an unidentified line. The radial velocities of the identified lines in Table 1 are velocities at the intensity peak. No recombination lines lie within the observed frequency ranges. We inspected the intensity maps of all detected molecular lines, but we did not find any extended features.

4. DISCUSSION

In this section we focus on the properties of the ^{12}CO $J = 6$–5 line. In particular, we discuss the structure probed by the ^{12}CO $J = 6$–5 line and the large missing flux of the low-velocity component of the ^{12}CO $J = 6$–5 line.

A notable finding in the present observation is that the cavity structure, which was found by the Sánchez Contreras observation in the ^{12}CO $J = 2$–1 line, is not clear in the ^{12}CO $J = 6$–5 maps, although the beam sizes are almost the same as those in the Sánchez Contreras observation. An immediate explanation for the missing cavity is that the emission of the ^{12}CO $J = 6$–5 line corresponding to the cavity wall is resolved out by the interferometry. However, we have to be careful in this interpretation,

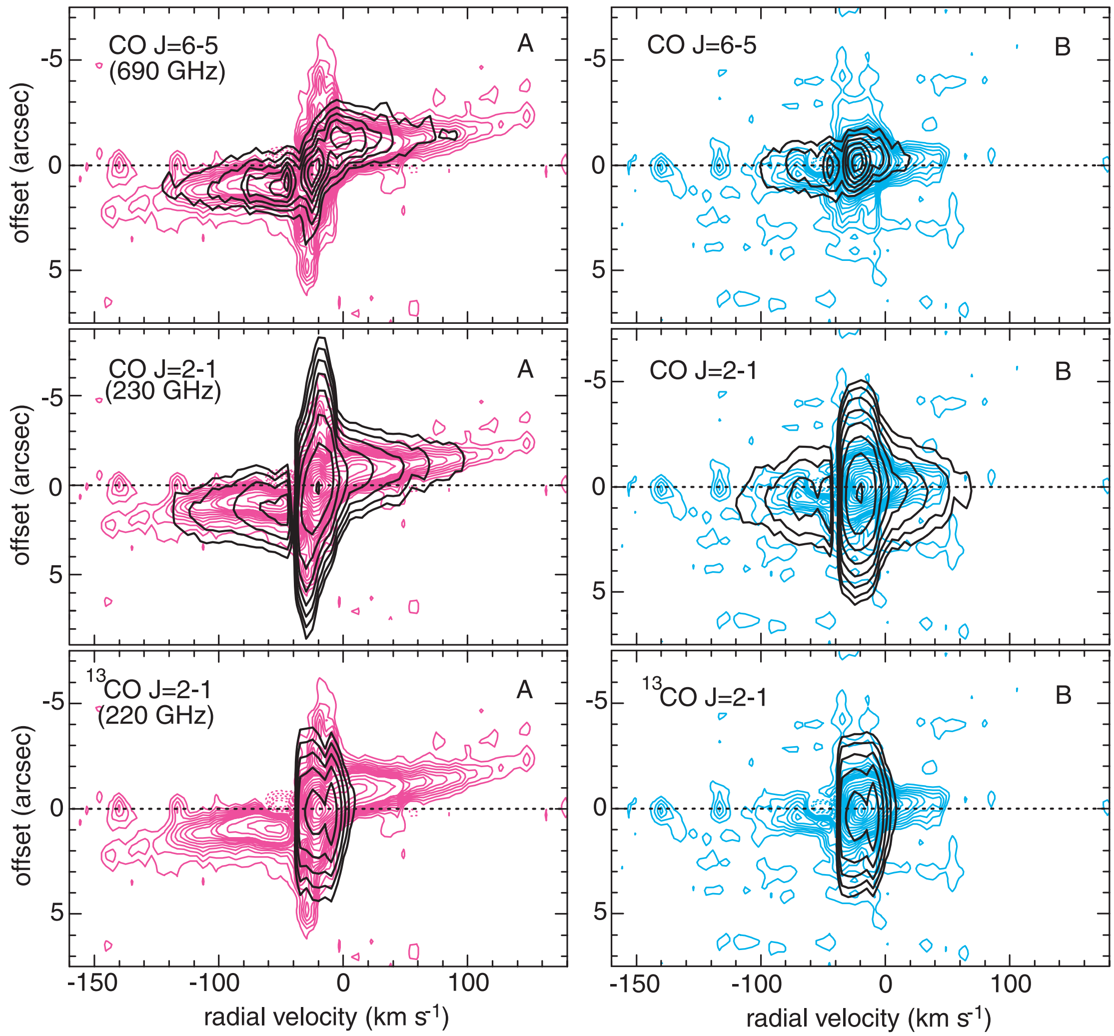

FIG. 8.—Position-velocity diagrams of the CO $J = 6$–5, CO $J = 2$–1, and ^{13}CO $J = 2$–1 lines superimposed on the similar diagram of the ^{12}CO $J = 2$–1 line taken from Sánchez Contreras et al. (2004). "A" and "B" refer to the direction of the cut indicated in Fig. 4. The contours start at the 3 σ level. A linear scale is used for the top panels, and the increment of the contours is 1.75 Jy beam^{-1}. A logarithmic scale is used for the middle and bottom panels. The dashed horizontal lines represent the origin of the offset axes.

because the cavity wall probed by the ^{12}CO $J = 2$–1 line has exhibited thin structure (thickness of $\sim 1''$).

In a careful second look at Figure 3, we realize that the features seen in the velocity-channel maps of ^{12}CO $J = 6$–5 seem to trace the south wall of the cavity, even though it is not very clear. In Figure 3, for example, the map at -26 km s^{-1} shows an extension to the east-southeast direction from the nebula center, and the map at -16 km s^{-1} shows an extension to the west-southwest direction from the nebula center. In addition, in Figure 4 (*bottom*) the intensity peak of the CO emission seems to be shifted ($\sim 0.8''$ to south) from the position of the continuum sources. These phenomena, presumably, suggest that we detected only the south wall of the cavity in the ^{12}CO $J = 6$–5 line, and that we did not detect the central dense core and the north wall of the cavity.

However, we still have a couple of questions: (1) What is the source of the missing flux of the ^{12}CO $J = 6$–5 line, and (2) why is only the north wall detectable in the ^{12}CO $J = 6$–5 line? In terms of the expanding velocity and the angular size of the structure, only the spherical halo and the slow axial component could be a possible source of the missing flux. The emission from the spherical halo is expected to be partially resolved out if it is detectable in the ^{12}CO $J = 6$–5 line, because the spherical halo is largely extended (at least, in the ^{12}CO $J = 2$–1 line). However, an important point is that we cannot expect the spherical halo to be highly excited enough to emit the ^{12}CO $J = 6$–5 line. The CO lines emitted from a circumstellar spherical halo are usually radiatively excited by infrared emission from the central star and the dust component in the envelope. (The energy input to the dust component originally comes from the central star. Therefore, we cannot expect strong IR emission in the outer part of the envelope even if we assume the IR emission to be from the dust.) Therefore, only the cavity wall (slow axial component) may be the possible source of the missing flux, at least, among the known components in the CRL 618 molecular envelope.

In the current scenario (Lee & Sahai 2003; Sánchez Contreras et al. 2004), the cavity wall is formed by an interaction between ambient material and the energetic high-velocity jet. The shock caused by the energetic jet would be a possible reason for a high temperature/density, which would excite the ^{12}CO $J = 6$–5 line. In fact, the Sánchez Contreras model, which has reasonably reproduced their observations in the CO and HC_3N lines, has applied 200 K as the temperature of the cavity wall. This temperature is much higher than the excitation temperature of the ^{12}CO $J = 6$–5 line ($\sim$100 K).

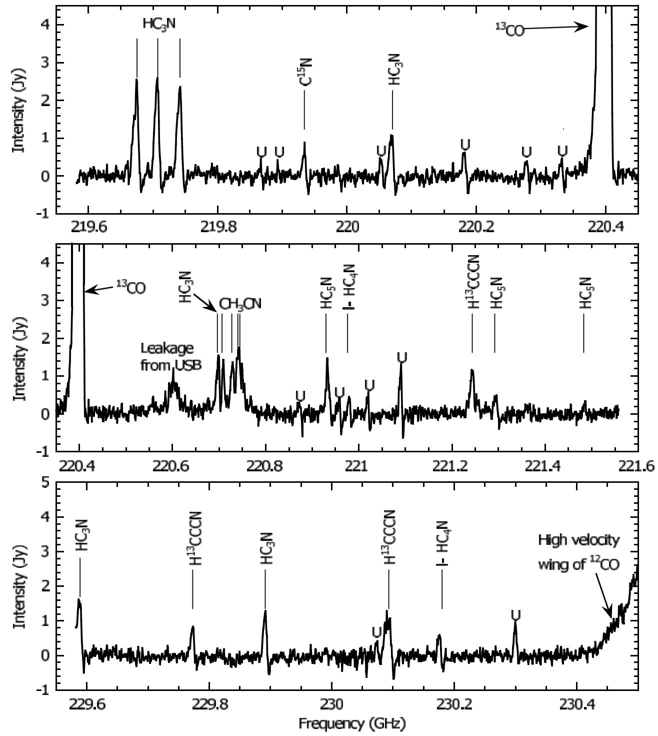

FIG. 9.—Spatially integrated spectra in the 1 mm band. The integrated area is the same as in Fig. 1. The horizontal axis represents the laboratory-frame frequency, corrected using $V_{lsr} = -23$ km s^{-1}. The vertical solid bars indicate the rest frequencies of identified lines. "U" means an unidentified line.

In our opinion, the following two reasons cause the absence of the north wall of the cavity. First, the temperature and/or density of the north wall are smaller than those of the south wall. Consequently, the north wall exhibits a weaker intensity in the ^{12}CO $J = 6$–5 line. In fact, the north wall shows a weaker intensity in the ^{12}CO $J = 2$–1 line (Sánchez Contreras et al. 2004). Second, the different *u-v* coverage between the Sánchez Contreras and the present observations possibly causes the missing northern cavity wall. The rate of the missing flux strongly depends on the pattern of the *u-v* coverage. In some cases an elongated structure could be resolved out even if it shows thin structure. Presumably, the missing northern cavity is a combination of these two effects. The difference in the temperature/density between the north and south walls, if it is real, leads to the fact that the physical conditions in the CRL 618 molecular envelope are not exactly axially symmetric. The southern part of the envelope (especially in the innermost part) may exhibit a relatively higher temperature/density compared with the northern part. This non–axially symmetric distribution of the temperature/density might be caused by the central star (for example, binarity and/or time variation of the post-AGB wind, which are very poorly understood).

5. SUMMARY

This paper has reported the results of an SMA observation of the proto–planetary nebula CRL 618 in the ^{12}CO $J = 6$–5 line. We also observed simultaneously in the ^{12}CO $J = 2$–1 and ^{13}CO $J = 2$–1 lines. In addition to the CO lines, we have detected a number of emission lines at 230 GHz. The main results are as follows:

1. The flux of the high-velocity component of the ^{12}CO $J = 6$–5 line is almost fully recovered, while we lost roughly 80% of the low-velocity component flux. This suggests that the emission region of the low-velocity component of the ^{12}CO $J = 6$–5 line is largely extended.

2. The existence of the cavity structure, which has been found in a previous observation in the ^{12}CO $J = 2$–1 line, is not clear in the ^{12}CO $J = 6$–5 maps. Only the south wall of the cavity seems to be detected in the ^{12}CO $J = 6$–5 line. This result suggests that the physical condition of the molecular envelope of CRL 618 is not exactly axially symmetric.

3. Continuum emission is detected at both 230 and 690 GHz. The flux of the 690 GHz continuum emission seems to be partially resolved out by the interferometry. This possibly suggests that dust emission significantly contaminates the 690 GHz continuum flux.

TABLE 1
LINE DETECTIONS

Frequency (MHz)	Species	Transition	V_{lsr} (km s^{-1})	S (Jy km s^{-1})
219675.114.....	HC_3N	$J = 24$–23, $\nu_7 = 2l = 0$	−22.0	26.3
219707.349.....	HC_3N	$J = 24$–23, $\nu_7 = 2l = 2e$	−22.1	25.4
219741.866.....	HC_3N	$J = 24$–23, $\nu_7 = 2l = 2f$	−23.1	25.1
219866.826.....	U		...	1.37
219892.538.....	U		...	1.13
219934.820.....	$C^{15}N$	$N = 2$–1, $J = 5/2$–3/2	−22.4	4.89
220050.478.....	U		...	2.89
220070.185.....	HC_3N	$J = 24$–23, $\nu_7 = 3l = 1e$	−20.2	10.1
220181.972.....	U		...	4.87
220278.206.....	U		...	2.54
220332.566.....	U		...	2.54
220398.681.....	^{13}CO	$J = 2$–1	−10.0	310.0
220699.688.....	HC_3N	$J = 24$–23, $\nu_7 = 3l = 1f$	−21.2	17.4
220709.024.....	CH_3CN	$J_K = 12_3$–11_3	−22.5	14.9
220730.266.....	CH_3CN	$J_K = 12_2$–11_2	−21.6	16.5
220743.015.....	CH_3CN	$J_K = 12_1$–11_1	−22.3	...
220747.265.....	CH_3CN	$J_K = 12_0$–11_0	−25.5	...
220868.094.....	U		...	2.60
220932.401.....	HC_5N	$J = 83$–82, $\nu = 0$	−23.5	15.8
220957.716.....	U		...	3.28
220979.090.....	l-HC_4N	$J = 48$–47	−22.9	3.08
221020.158.....	U		...	3.34
221090.680.....	U		...	8.77
221246.240.....	$H^{13}CCCN$	$J = 25$–24, $\nu_7 = 1l = 1e$	−18.3	19.8
221295.423.....	HC_5N	$J = 83$–82, $\nu_{11} = 1l = 1f$	−23.3	5.15
221486.033.....	HC_5N	$J = 83$–82, $\nu_{11} = 1l = 1e$	−22.8	2.42
229589.088.....	HC_3N	$J = 25$–24, $\nu_7 = 3l = 3f$	−19.9	16.5
229772.876.....	$H^{13}CCCN$	$J = 26$–25, $\nu_7 = 1l = 1e$	−23.7	6.61
229891.277.....	HC_3N	$J = 25$–24, $\nu_7 = 3l = 1e$	−23.6	9.46
230074.654.....	U		...	2.19
230093.224.....	$H^{13}CCCN$	$J = 26$–25, $\nu_7 = 1l = 1f$	−18.8	14.6
230180.393.....	l-HC_4N	$J = 50$–49	−17.4	4.04
230299.796.....	U		...	5.81
230538.000.....	CO	$J = 2$–1	−20.0	1541.4
690552.098.....	$H^{13}CN$	$J = 8$–7	−19.6	346.4
691473.076.....	CO	$J = 6$–5	−22.0	4647.8

We are grateful to Rob Christensen, Alison Peck, and the SMA team for making the 690 GHz campaign possible. This research has been supported by the Academia Sinica Institute of Astronomy and Astrophysics and the Smithsonian Institute, and has made use of the SIMBAD and ADS databases. The authors thank Jinhua He, Holger Müeller, and Shuro Takano for their help in the identification of the molecular lines. J. N. thanks Paul Ho for his constant encouragement.

REFERENCES

Balick, B., & Frank, A. 2002, ARA&A, 40, 439
Bujarrabal, V., Alcolea, J., Neri, R., & Grewing, M. 1994, ApJ, 436, L169
Bujarrabal, V., Castro-Carrizo, A., Alcolea, J., & Sánchez Contreras, C. 2001, A&A, 377, 868
Bujarrabal, V., Gómez-González, J., Bachiller, R., & Martín-Pintado, J. 1988, A&A, 204, 242
Cernicharo, J., Guelin, M., Martín-Pintado, J., Penalver, J., & Mauersberger, R. 1989, A&A, 222, L1
Cernicharo, J., Heras, A. M., Tielens, A. G. G. M., Pardo, J. R., Herpin, F., Guelin, M., & Waters, L. B. F. M. 2001a, ApJ, 546, L123
Cernicharo, J., et al. 2001b, ApJ, 546, L127
Fukasaku, S., Hirahara, Y., Masuda, A., Kawaguchi, K., Ishikawa, S., & Kaifu, N. 1994, ApJ, 437, 410
García-Segura, G., Lopez, J. A., & Franco, J. 2005, ApJ, 618, 919
Goodrich, R. W. 1991, ApJ, 376, 654
Hajian, A. R., Phillips, J. A., & Terzian, Y. 1996, ApJ, 467, 341
Herpin, F., Goicoechea, J. R., Pardo, J. R., & Cernicharo, J. 2002, ApJ, 577, 961
Ho, P., Moran, J. M., & Lo, K. Y. 2004, ApJ, 616, L1
Jura, M., & Chen, C. 2000, ApJ, 544, L141
Knapp, G. R., Sandell, G., & Robson, E. I. 1993, ApJS, 88, 173
Kwok, S. 1993, ARA&A, 31, 63
———. 2004, Nature, 430, 985
Kwok, S., & Bignell, R. C. 1984, ApJ, 276, 544
Kwok, S., & Feldman, P. A. 1981, ApJ, 247, L67
Lee, C., & Sahai, R. 2003, ApJ, 586, 319
Lucas, R., Omont, A., Guilloteau, S., & Nguyen-Q-Rieu. 1986, A&A, 154, L12
Martín-Pintado, J., Gaume, R., Bachiller, R., & Johnson, K. 1993, ApJ, 419, 725
Meixner, M., Campbell, M. T., Welch, W. J., & Likkel, L. 1998, ApJ, 509, 392
Morris, M., Guilloteau, S., Lucas, R., & Omont, A. 1987, ApJ, 321, 888
Müller, H. S. P., Schloder, F., Stutzki, J., & Winnewisser, G. 2005, J. Molecular Structure, 742, 215
Müller, H. S. P., Thorwirth, S., Roth, D. A., & Winnewisser, G. 2001, A&A, 370, L49
Murakawa, K., Nakashima, J., Ohnaka, K., & Deguchi, S. 2007, A&A, 470, 957
Nakashima, J., & Deguchi, S. 2000, PASJ, 52, L43
———. 2004, ApJ, 610, L41
———. 2005, ApJ, 633, 282
Neri, R., Garcia-Burillo, S., Guelin, M., Guilloteau, S., & Lucas, R. 1992, A&A, 262, 544
Ohashi, N. 2005, J. Korean Astron. Soc., 38, 103
Pardo, J. R., & Cernicharo, J. 2007, ApJ, 654, 978
Pardo, J. R., Cernicharo, J., Goicoechea, J. R., & Phillips, T. G. 2004, ApJ, 615, 495
Pearson, J. C., Drouin, B. J., & Pickett, H. M. 2005, in IAU Symp. 235, Galaxy Evolution across the Hubble Time, ed. F. Combes & J. Palouš (New York: Cambridge Univ. Press), 270
Remijan, A., Wyrowsky, F., Friedel, D. N., Meier, D. S., & Snyder, L. E. 2005, ApJ, 626, 233
Sánchez Contreras, C., Bujarrabal, V., Castro-Carrizo, A., Alcolea, J., & Sargent, A. 2004, ApJ, 617, 1142
Sánchez Contreras, C., & Sahai, R. 2004, ApJ, 602, 960
Sault, R. J., Teuben, P. J., & Wright, M. C. H. 1995, in ASP Conf. Ser. 77, Astronomical Data Analysis Software and Systems IV, ed. R. A. Shaw, H. E. Payne, & J. J. E. Hayes (San Francisco: ASP), 433
Shibata, K. M., Deguchi, S., Hirano, N., Kameya, O., & Tamura, S. 1993, ApJ, 415, 708
Steffen, W., Lopez, J. A., & Lim, A. 2001, ApJ, 556, 823
Szczerba, R., Siodmiak, N., Stasinska, G., & Borkowski, J. 2007, A&A, 469, 799
Trammell, S. R., & Goodrich, R. W. 2002, ApJ, 579, 688
van Winckel, H. 2003, ARA&A, 41, 391
Wynn-Williams, C. G. 1977, MNRAS, 181, P61
Wyrowski, F., Schilke, P., Thorwirth, S., Menten, K. M., & Winnewisser, G. 2003, ApJ, 586, 344
Yamamura, I., Shibata, K. M., Kasuga, T., & Deguchi, S. 1994, ApJ, 427, 406